Geoscience Frontiers 12 (2021) 101251

HOSTED BY

Contents lists available at ScienceDirect

Geoscience Frontiers

journal homepage: www.elsevier.com/locate/gsf

Research Paper

Modifications in aerosol physical, optical and radiative properties during heavy aerosol events over Dushanbe, Central Asia

Dipesh Rupakheti [a], Maheswar Rupakheti [b], Xiufeng Yin [a], Julian Hofer [c], Mukesh Rai [a], Yuling Hu [a], Sabur F. Abdullaev [d], Shichang Kang [a,e,*]

[a] State Key Laboratory of Cryospheric Science, Northwest Institute of Eco-Environment and Resources, Chinese Academy of Sciences, Lanzhou 730000, China
[b] Institute for Advanced Sustainability Studies, Potsdam, Germany
[c] Leibniz Institute for Tropospheric Research, Leipzig, Germany
[d] Physical Technical Institute of the Academy of Sciences of Tajikistan, Dushanbe, Tajikistan
[e] Center for Excellence in Tibetan Plateau Earth Sciences, Chinese Academy of Sciences, Beijing 100101, China

ARTICLE INFO

Article history:
Received 26 April 2021
Revised 3 June 2021
Accepted 15 June 2021
Available online 18 June 2021
Handling Editor: M. Santosh

Keywords:
Dust events
Aerosol optical properties
AERONET
Dushanbe
Central Asia

ABSTRACT

The location of Central Asia, almost at the center of the global dust belt region, makes it susceptible for dust events. The studies on atmospheric impact of dust over the region are very limited despite the large area occupied by the region and its proximity to the mountain regions (Tianshan, Hindu Kush-Karakoram-Himalayas, and Tibetan Plateau). In this study, we analyse and explain the modification in aerosols' physical, optical and radiative properties during various levels of aerosol loading observed over Central Asia utilizing the data collected during 2010–2018 at the AERONET station in Dushanbe, Tajikistan. Aerosol episodes were classified as strong anthropogenic, strong dust and extreme dust. The mean aerosol optical depth (AOD) during these three types of events was observed a factor of ~3, 3.5 and 6.6, respectively, higher than the mean AOD for the period 2010–2018. The corresponding mean fine-mode fraction was 0.94, 0.20 and 0.16, respectively, clearly indicating the dominance of fine-mode anthropogenic aerosol during the first type of events, whereas coarse-mode dust aerosol dominated during the other two types of events. This was corroborated by the relationships among various aerosol parameters (AOD vs. AE, and EAE vs. AAE, SSA and RRI). The mean aerosol radiative forcing (ARF) at the top of the atmosphere (ARF_{TOA}), the bottom of the atmosphere (ARF_{BOA}), and in the atmosphere (ARF_{ATM}) were −35 ± 7, −73 ± 16, and 38 ± 17 Wm^{-2} during strong anthropogenic events, −48 ± 12, −85 ± 24, and 37 ± 15 Wm^{-2} during strong dust event, and −68 ± 19, −117 ± 38, and 49 ± 21 Wm^{-2} during extreme dust events. Increase in aerosol loading enhanced the aerosol-induced atmospheric heating rate to 0.5–1.6 K day^{-1} (strong anthropogenic events), 0.4–1.9 K day^{-1} (strong dust events) and 0.8–2.7 K day^{-1} (extreme dust events). The source regions of air masses to Dushanbe during the onset of such events are also identified. Our study contributes to the understanding of dust and anthropogenic aerosols, in particular the extreme events and their disproportionally high radiative impacts over Central Asia.

1. Introduction

Dust aerosols in the atmosphere influence the Earth's climate system through scattering and absorption of the radiation, modification in cloud microphysical properties, melting of snowfields and glaciers among many other impacts (IPCC, 2013; Huang et al., 2014). About one-third of the earth's land surface is occupied by arid and semi-arid regions, which are the primary sources of dust with about 1000–3000 Tg per year of dust entrained into the atmosphere from these regions (Penner, 2001; Huang et al., 2010, 2014). Such dust particles in the atmosphere influence not only the climate but, once deposited, act as essential nutrients for ecosystem productivity both in land and ocean (Mahowald et al., 2009; Prospero et al., 2010), alter the albedo of snow and ice surface (Kaspari et al., 2014; Zhang et al., 2018) and contribute to the soil development (Muhs et al., 2007). The arid and desert regions are the main source of dust where the particles with diameter as large as 100 μm are found but only those particles with diameter < 10 μm are transported over thousands of kilometers

* Corresponding author at: State Key Laboratory of Cryospheric Science, Northwest Institute of Eco-Environment and Resources, CAS, Donggang West Rd. 320, Lanzhou 730000, China.
E-mail address: shichang.kang@lzb.ac.cn (S. Kang).

https://doi.org/10.1016/j.gsf.2021.101251
1674-9871/

downwind from the source regions (Miller et al., 2004; Seinfeld and Pandis, 2016). Among the desert regions, the North African deserts have the highest share (~50%–70%) in atmospheric dust, followed by the Asian deserts (~10%–25%) (Tegen and Schepanski, 2009) and remaining contributions from Arabia, Australia, southern Africa and American drylands (e.g., Middleton, 2017). Additionally, the total dust emission from the northern hemisphere is almost 15 times higher (~1935 Mt yr^{-1}) than from the southern hemisphere (138 Mt yr^{-1}) (Ginoux et al., 2004).

Central Asia, compromising of five countries viz. Kazakhstan, Kyrgyzstan, Tajikistan, Uzbekistan and Turkmenistan, lies almost at the center of the global dust belt extending from the Sahara in northern Africa through the Arabian deserts and Taklamakan Desert up to the Gobi Desert (Hofer et al., 2017). Dust from northern Africa and the northern Arabian Peninsula is transported towards the Central Asian region because of strong southwesterly winds and the development of low-pressure systems over the western part of Siberia (Liu et al., 2019). The regional dust, along with local dust and anthropogenic aerosols that originate over the Central Asian region, are further transported by westerlies towards the mountain ranges like the Tian Shan, the Hindu Kush-Karakoram-Himalayas and the Tibetan Plateau (Kang et al., 2019). These mountain ranges, situated in the proximity of Central Asia, are called as the 'water towers of the world'. Nearly 1.5 billion people within and downstream of these mountain regions are dependent on those mountains as the source of freshwater (Immerzeel et al., 2010). The dust and anthropogenic aerosols affect the sensitive ecosystems including the cryosphere (Kang et al., 2019). There are some recent studies on the emission of dust, its variation and trend in Central Asia (Xi and Sokolik, 2015, 2016a, 2016b). Among the limited available studies from this region, Issanova and Abuduwaili (2017) provided an overview on the status of dust storms, their frequency, spatiotemporal distribution and relation with land degradation, regional division and aeolian transport. A couple of other studies used satellite observations to investigate the aerosol optical depth (AOD) over the Central Asian region (Kumar et al., 2018; Rupakheti et al., 2019a; Liu et al., 2020; Wang et al., 2020; Zhang et al., 2020) while three recent studies analyzed aerosol optical properties and estimated their radiative impacts over Dushanbe (the capital city of Tajikistan) using columnar aerosol observations at the NASA AERONET site at Dushanbe site using a sunphotometer (Abdullaev et al., 2014; Rupakheti et al., 2020b), a Raman Lidar, including cases of heavy aerosol loading during 2015–2016 (Hofer et al.,2017)

Nevertheless, though the region is frequently hit by dust storms, studies on the modification of aerosol physical, optical and radiative properties during the occurrence of dust storms over the Central Asian region are still very limited. Therefore, this study has been conducted with an aim to provide a general overview on the physical and optical characteristics of aerosols with a special focus on aerosol characteristics and source identification during several episodes with (i) dust events and (ii) anthropogenic air pollution events that occurred over Dushanbe, Tajikistan during 2010–2018. We believe that the (previously unavailable) data reported here are extremely valuable considering the vastness of the Central Asia, its proximity to regions with sensitive ecosystems, and the lack of monitoring and scientific study of the issue in the region.

2. Methods

2.1. Study site

Tajikistan, the smallest country in Central Asia, with an area of about 143 thousand km^2, shares its border with Kyrgyzstan (north), China (east), Uzbekistan (west) and Afghanistan (south), and has dry continental climate (Abdullaev and Sokolik, 2019; Hofer et al., 2020). It is a mountainous country with more than 93% of the total land covered by mountains and with more than a half of the total land situated at elevations higher than 3000 m a.s.l., resulting in a very low proportion of land available for agricultural purpose (Abdullaev et al., 2019). As a mountain valley and region with high economic activities in the country, the air quality of Dushanbe is influenced by anthropogenic activities. Additionally, as this region is located in proximity to the desert regions, it gets often affected by the dust from the deserts (Abdullaev et al., 2014; Hofer et al., 2017; Rupakheti et al., 2019a, 2020b).

2.2. AERONET data

A ground-based CIMEL Sun/sky radiometer was installed in Dushanbe (Fig. 1) in June 2010, as a part of the NASA AERONET (AErosol Robotic NETwork) program, with an aim to contribute to the understanding of aerosol optical and radiative properties over this important region. The CIMEL sunphotometer measures the direct-sun irradiance in eight channels between 340 and 1020 nm and sky radiance in four channels between 440 and 1020 nm (Holben et al., 1998, 2001). We have used version 3 level 2 (cloud screened and quality assured) data (Giles et al., 2019) as available on the AERONET website (https://aeronet.gsfc.nasa.gov/). Among various data available, we have used AOD, Ångström exponent (AE), volume size distribution (VSD), single scattering albedo (SSA), asymmetry parameter (ASY), and refractive index (RI). AE is an important parameter that describes how AOD typically depends on the wavelength of the light, and it is calculated as (Holben et al., 2001), Eq.(1):

$$\alpha = -\frac{\log\left(\frac{\tau_1}{\tau_2}\right)}{\log\left(\frac{\lambda_1}{\lambda_2}\right)} \quad (1)$$

where τ_1 and τ_2 are AOD at wavelength λ_1 and λ_2, respectively. AE is inversely proportional to the aerosol size; low AE indicates presence of coarse particles like dust and sea-salt, and high AE, fine particles from combustion processes.

In this study, the radiative forcing data available from the AERONET website has also been used to study the influence of aerosol loading on the energy balance. Over different types of landforms like urban-industrial, biomass burning, mineral dust, background continental, maritime aerosols and free troposphere, the solar fluxes measured by AERONET sunphotometers correlated well with the ground-based observations (García et al., 2008). More details on the AERONET observations, data processing and uncertainties have been discussed in earlier studies (Smirnov et al., 2000; Holben et al., 2001; Garcia et al., 2008). The operational AERONET ARF_{BOA} (aerosol radiative forcing at the bottom/-surface of the atmosphere) is corrected for effects of surface albedo by multiplying it with (1-SA), where SA is the spectral average surface albedo of the site (Garcia et al., 2008; Ramachandran and Rupakheti, 2020), and it was 0.23 ± 0.03 for the Dushanbe site for the period 2010–2018.

2.3. Classification of 'heavy aerosol' events

Earlier studies have proposed that the aerosol events can be categorized utilizing the AOD data. For example; dust events over the Mediterranean region have been classified as strong aerosol events if AOD during the event is ≥ mean AOD + (2 × standard deviation) and extreme aerosol events if AOD ≥ mean AOD + (4 × standard deviation) (Gkikas et al., 2009, 2013, 2016). Using the same classification technique, Hofer et al. (2017) investigated extreme dust

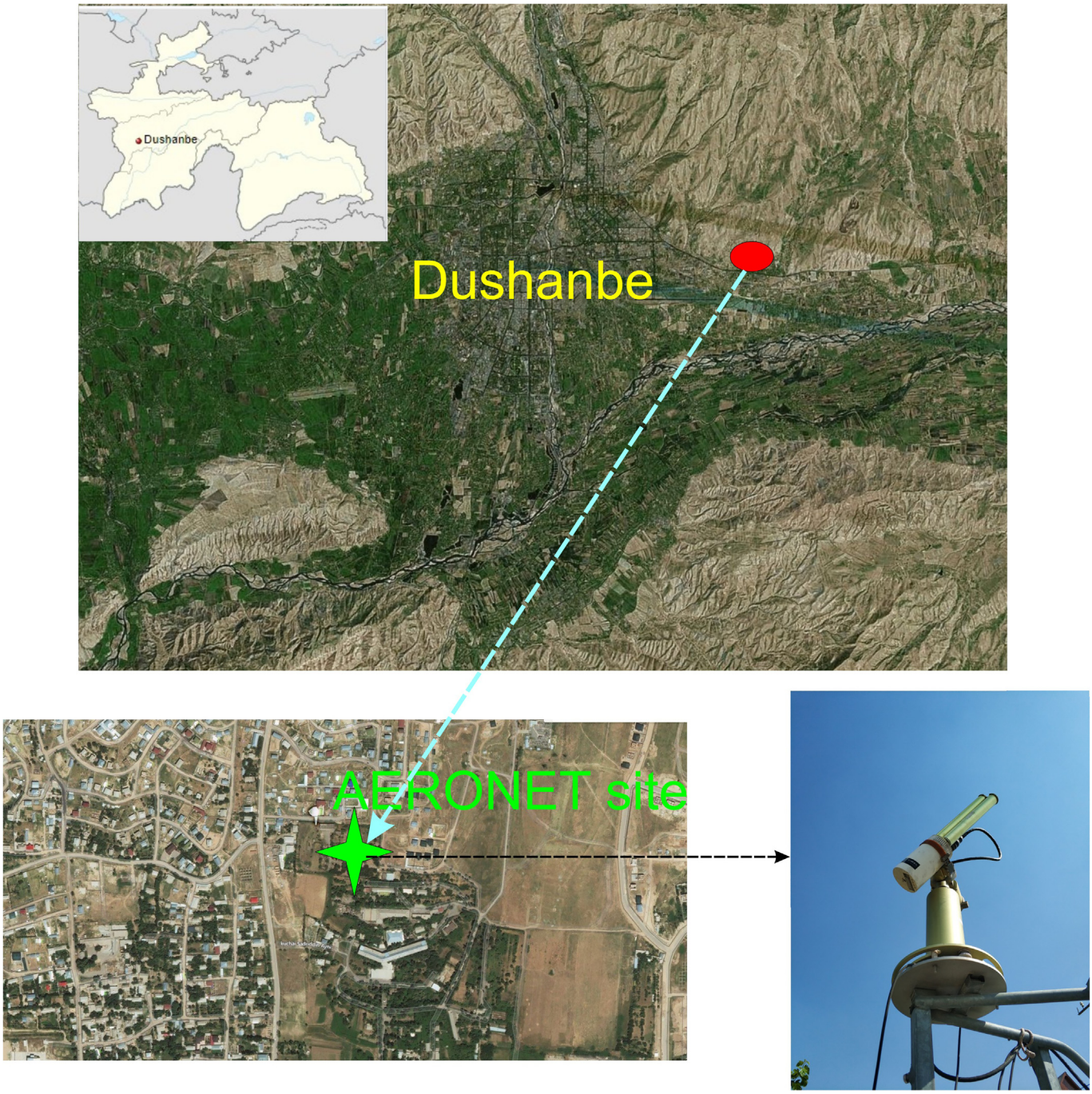

Fig. 1. Location of AERONET site in Dushanbe (red oval marker) and the zoomed image showing the surrounding (obtained from Bing Maps at https://www.bing.com/maps) with a Cimel sunphotometer in action at the site.

events observed over Dushanbe during 2015–2016. We also followed the same criteria for categorization of aerosol events into extreme dust, strong dust and strong anthropogenic (a short form 'strong anthro' is used in the figures) events. The strong anthropogenic event category is classified based on the same criteria and values for AOD as in case of strong dust but with high AE values, which are associated with small particles, mainly from combustion of fossil fuel and biomass. The mean AOD during the whole study period (2010–2018) was 0.28 ± 0.20 (Rupakheti et al., 2020b). This resulted in identification of strong dust events on days with AOD $\geq$ 0.68 and extreme dust events on days with AOD $\geq$ 1.08. Out of 1626 days of available level 2 data, 16 days observed extreme dust events whereas 26 days were with strong dust events. Ten days out of the 26 days with strong dust events were classified as strong anthropogenic event days because AE values on those days were high, in 1.05–1.43 range. However, AERONET inversion products (e.g., SSA) (Holben et al., 2001) were available only for 13 days each for extreme dust events and strong dust events, and only for 4 days for strong anthropogenic events. This study utilized those data only. To understand the evolution and regional extent of the aerosol loadings during the events, we used the MODIS-Terra imageries during the event days as available from the NASA Worldview Snapshots (https://wvs.earthdata.nasa.gov/) (Supplementary Data, Fig. S1–S3).

2.4. Air mass back-trajectories during the events

The routes of air mass transport were studied in order to understand the source regions of those air masses that carried aerosol along to Dushanbe. For this purpose, we analyzed the origins and paths of hourly trajectories of air masses for 120 h prior to the events (back trajectories) that arrived at 500 m (above the ground) over the Dushanbe site. Additionally, we studied the air mass pathways for 24 h prior to the onset of events. We used the Hybrid Single-Particle Lagrangian Integrated Trajectory (HYSPLIT) back-trajectory model (Draxler and Hess, 1998; Stein et al., 2015) with $1 \times 1^{\circ}$ meteorological data from Global Data Assimilation System (GDAS) for calculating the trajectories and TrajStat plugin of MeteoInfo (Wang, 2014) for plotting those trajectories.

We used ERA5 reanalysis wind data to study the synoptic scale circulation before, during and after the events for which we selected only the days with highest aerosol loading for each event types. The data were retrieved from the Copernicus Climate Data Store (https://cds.climate.copernicus.eu/) platform. Description on the ERA5 and related data products could be accessed elsewhere (Hersbach et al., 2020).

3. Results and discussion

3.1. Aerosol loading and AE during aerosol events

The mean AODs and AEs for all four cases (extreme dust events, strong dust events, strong anthropogenic events, and 2010–2018 (all data but event days)) are presented in Fig. 2 where the lowest AOD during the 2010–2018 can be observed. The mean (±standard deviation) AOD and AE during the 2010–2018 were 0.25 ± 0.12 and 0.83 ± 0.39, respectively, with almost a half of the AOD was contributed by the fine-mode particles as the average fine-mode fraction (FMF: fraction of total AOD contributed by the fine mode particles) was 0.52 ± 0.20. In a recent study, the mean AOD and AE during 2010–2018 (considering all data) over Dushanbe were reported as 0.28 ± 0.20 and 0.82 ± 0.40, respectively (Rupakheti et al., 2020b). The lowest AE (average: 0.09 ± 0.06) with the highest AOD (average: 1.64 ± 0.56) and the lowest FMF (average: 0.16 ± 0.04) during the extreme dust events (Table 1) indicate the presence of coarse-mode dust aerosols in Dushanbe's atmosphere on those days. During the strong dust events, mean AOD (0.88 ± 0.10) was almost a half of that during the extreme dust events with a bit higher mean AE and mean FMF (0.16 ± 0.09 and 0.20 ± 0.05, respectively). Regarding the strong anthropogenic events, even though the mean AOD (0.74 ± 0.06) was lower than earlier two type of events, the AE values were 14 and 8 times higher than earlier cases with average FMF of 0.94 ± 0.02 indicating a clear dominance of fine aerosols mostly sourced from anthropogenic activities like urban/industrial activities or biomass burning.

The relationship between AOD and AE, which is a most common method to investigate aerosol types (Kaskaoutis et al., 2007; Iftikhar et al., 2018; Rupakheti et al., 2018, 2020a, 2020b), confirms the aerosol types during different events (Fig. 3a). In this study, we have utilized the same thresholds of AOD and AE for the classification of aerosol types that we adopted in our recent studies over Central Asia (Rupakheti et al., 2019a, 2020b) which led to a clear clustering of aerosol types into (i) dust, (ii) urban/industrial (U/I), and (iii) biomass burning (BB) aerosols. The contributions of U/I and BB aerosols were found highest during winter followed, in decreasing order, by autumn and spring and summer whereas the dust aerosol followed exactly opposite pattern, highest in summer and lowest in winter (Rupakheti et al., 2020b). During 2010–2018 (all data), the share of dust aerosol was 2.71% (Rupakheti et al., 2020b). Additionally, the relationship among other parameters, such as absorption Ångström exponent (AAE) vs. extinction Ångström exponent (EAE), SSA vs. EAE, and real refractive index (RRI) vs. EAE, was plotted using the threshold values mentioned in earlier studies (Russell et al., 2010, 2014; Giles et al., 2012; Rupakheti et al., 2019b; Ramachandran and Rupakheti, 2020). Fig. 3b–d represents relation between various parameters, which further confirms the presence of dust aerosols during extreme dust and strong dust events and pollution aerosols from BB and U/I activities during strong anthropogenic events.

3.2. Size distribution, volume concentration and effective radius of aerosols during aerosol events

The volume size distribution (VSD) was derived from the sun-photometer measurements under 22 different radius size bins of particles from 0.05 to 15 μm. Bi-modal distribution of the aerosol VSD can be defined by the sum of two lognormal distributions as governed by Eq.(2) (Dubovik and King, 2000):

$$v(r) = \frac{dV(r)}{d\ln r} = \sum_{i=1}^{2} \frac{C_{v,i}}{\sqrt{2\pi}\sigma_i} \exp\left[\frac{-(\ln r - \ln r_{v,i})}{2\sigma_i^2}\right] \quad (2)$$

where, $C_{v,i}$ is the volume concentration for fine mode and coarse mode, σ_i is the geometric standard deviation for mode i, and $r_{v,i}$ is the volume mean radius.

Generally, the aerosols over Dushanbe have bi-modal volume size distribution (VSD) with a clear dominance of coarse-mode aerosols during summer and autumn which is 3–4 times higher as compared to the other two seasons (Rupakheti et al., 2020b). The aerosol VSD in the size range 0.05–15 μm radius for various event scenarios is presented in Fig. 4a. Excluding the aerosol events, i.e., for 2010–2018, the VSD was still bi-modal with modal peak at 3.86 μm and contribution at coarse-mode ~ 5 times higher than at the modal peak in fine-mode. In the case of strong anthropogenic events, the VSD was dominated by the fine-mode aerosols with modal peak at 0.15 μm. In the case of both extreme dust and strong dust events, the VSD was unimodal with the modal peak at 2.24 μm and peak values of 1.13 and 0.6, respectively. The modal peak observed (at 2.24 μm) during extreme dust events were higher by a factor of ~ 14, ~2, ~38 than that for 2010–2018, strong dust and strong anthropogenic events, respectively.

During 2010–2018 and strong anthropogenic events, the share of fine (coarse) mode aerosol volume concentration to the total volume concentration was 14% (86%) and 69% (31%), respectively (Fig. 4b). However, the remaining two types of events possessed different share: 6% (94%) during extreme dust and 8% (92%) during the strong dust events. The V_c/V_f ratio (coarse-mode particle volume to fine-mode particle volume) was as high as ~50 in the dust from western part of Africa and the Arabian Peninsula, and ~10 in aerosols from Bahrain-Persian Gulf (Dubovik et al., 2002). In our case, the V_c/V_f ratio was 16, 12, 6 and 0.46 for the extreme dust events, strong dust events, 2010–2018, and strong anthropogenic events, respectively, clearly indicating the higher amounts of coarse-mode aerosols during extreme dust events and strong dust events in Dushanbe as compared to the Bahrain-Persian Gulf. The effective radius (R_{eff}) of fine-mode aerosols remained more or less similar (between 0.1 and 0.2) but the variation in R_{eff} in coarse-mode was large with the values of 1.94, 1.95, 2.30 and 2.54 for extreme dust, strong dust, 2010–2018, and strong anthropogenic events, respectively. Rupakheti et al. (2020b) reported the highest value of R_{eff} during winter season (as compared with other seasons) as the share of anthropogenic aerosols sourced from urban/industrial and biomass burning was highest. In addition, owing to the increase in volume concentration in coarse-mode (with reduction in AE), the R_{eff} of total aerosol increased considerably

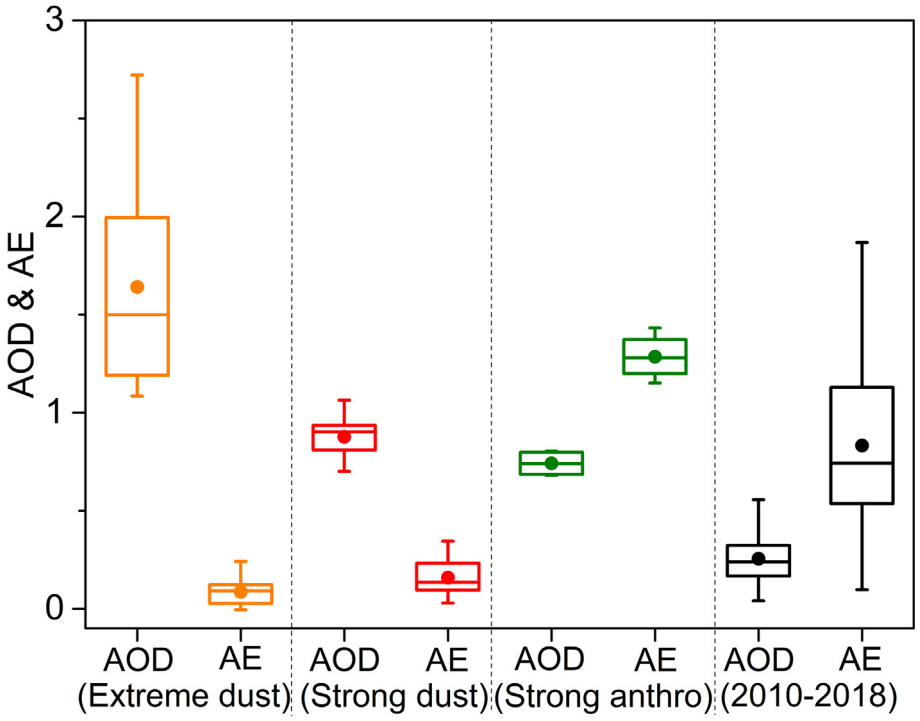

Fig. 2. Variation in AOD and AE during four cases of aerosol events during observation period 2010–2018: extreme dust events, strong dust events and strong anthropogenic aerosols events, and '2010–2018 (all data except that for those three types of events). In each box, the lower and upper boundary represent the 25th and 75th percentile, the top and bottom of the whisker represent the 90th and 10th percentile, the mid-line represents the median; and the filled circle represents the mean value.

Table 1
Daily mean AOD, AE and FMF during the extreme dust, strong dust and strong anthropogenic events.

Date	Event number	AOD	AE	FMF
Extreme dust				
23/08/2010	Event-1	2.71	0.12	–
13/10/2010	Event-2	1.60	0.06	0.14
22/10/2010	Event-3	1.08	0.03	0.13
08/08/2011	Event-4	1.75	0.10	0.17
26/08/2011	Event-5	2.06	0.14	0.21
04/09/2012	Event-6	1.09	0.11	0.17
02/07/2014	Event-7	1.50	0.12	0.17
28/09/2014	Event-8	1.10	0.08	0.15
06/07/2015	Event-9	1.19	0.09	0.18
15/07/2016	Event-10	2.72	−0.01	–
16/07/2016	Event-11	1.29	0.02	0.12
28/07/2016	Event-12	1.25	0.24	0.24
01/10/2016	Event-13	1.99	0.02	0.11
	Average	1.64 ± 0.56	0.09 ± 0.06	0.16 ± 0.04
Strong dust				
24/08/2010	Event-1	0.93	0.09	–
09/08/2011	Event-2	0.83	0.15	0.20
25/08/2011	Event-3	0.70	0.34	0.28
08/10/2011	Event-4	0.90	0.06	0.13
13/07/2012	Event-5	1.06	0.13	0.20
25/08/2012	Event-6	0.99	0.13	0.18
19/09/2014	Event-7	0.91	0.23	0.23
07/07/2015	Event-8	0.75	0.14	0.19
11/10/2015	Event-9	1.00	0.18	0.20
31/05/2017	Event-10	0.90	0.05	0.15
11/07/2017	Event-11	0.85	0.24	0.23
19/10/2017	Event-12	0.81	0.03	0.12
09/12/2017	Event-13	0.75	0.28	0.26
	Average	0.88 ± 0.10	0.16 ± 0.09	0.20 ± 0.05
Strong anthropogenic				
13/11/2014	Event-1	0.69	1.43	0.96
18/11/2017	Event-2	0.79	1.25	0.98
15/12/2017	Event-3	0.68	1.31	0.92
09/01/2018	Event-4	0.80	1.15	0.93
	Average	0.74 ± 0.06	1.29 ± 0.10	0.94 ± 0.02

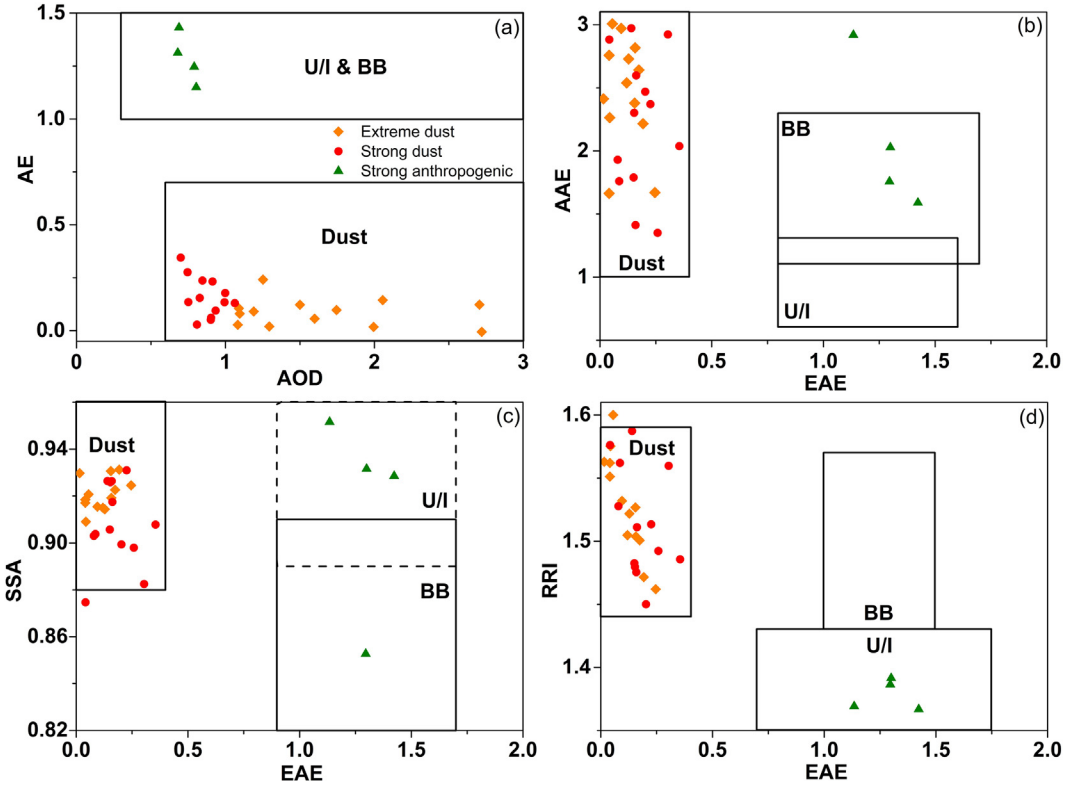

Fig. 3. Relationship between AOD and AE (a), AAE and EAE (b), SSA and EAE (c), and RRI and EAE (d) confirming the aerosol types during three types of events. U/I and BB refer to aerosols of Urban/industrial and Biomass burning origin, respectively.

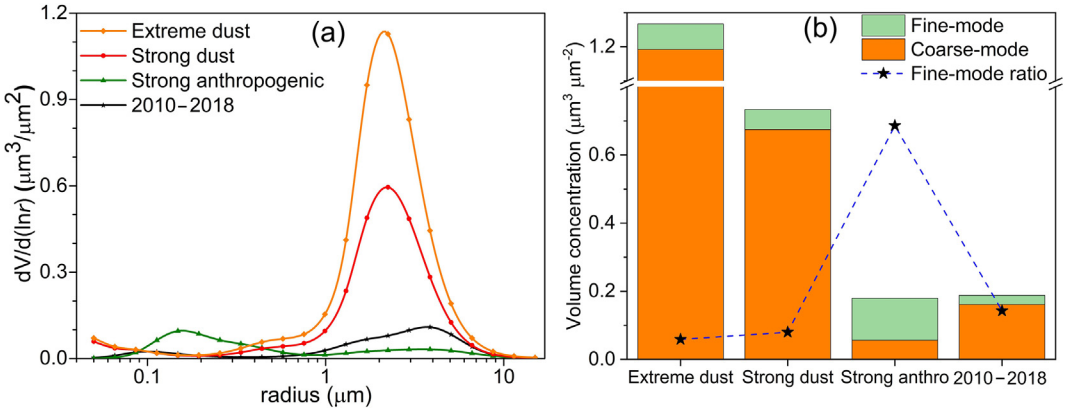

Fig. 4. Aerosol volume size distribution (a) and volume concentration (b) during various types of aerosol events observed over Dushanbe during 2010–2018.

(~3.7 and ~3.2 times) during extreme dust events and strong dust events, respectively, than with strong anthropogenic events. The values reported here are within the range reported in Dubovik et al. (2002) where the coarse-mode effective radii for U/I and BB emissions were higher than the dust influenced sites, whereas the fine-mode R_{eff} were almost similar (Dubovik et al., 2002).

3.3. SSA, ASY, and refractive index during aerosol events

The SSA is the fraction of scattering in the total extinction with values up to close to 1 for scattering aerosols like sulfate and lower values for the absorbing aerosols like soot (Pandithurai et al., 2008). In the case of dust aerosol, SSA increases with wavelengths whereas it is opposite for black carbon (BC) aerosols, and mixed aerosols show different spectral dependencies with wavelengths (Dubovik et al., 2002; Bergstrom et al., 2007; Russell et al., 2010). Fig. 5 (a) shows the spectral variation of average SSA with wavelength for various cases where we can notice the lowest values of SSA at shorter wavelengths because of larger absorption of light by dust particles in the UV or near-UV region of the spectrum (Dubovik et al., 2002; Kumar et al., 2015). As compared to the 2010–2018 case, we can notice an enhancement in the scattering occurred during the aerosol episodes with the highest scattering across all wavelengths during the extreme dust events (yellow color line in Fig. 5a). A similar feature of SSA has been reported over other regions across Asia during the dust events (Prasad et al., 2007; Pandithurai et al., 2008; Yu et al., 2013; Alam et al., 2014; Srivastava et al., 2014; Kumar et al., 2015; Iftikhar et al., 2018; Tiwari et al., 2019). The average SSA at 675 nm (SSA_{675}) over Dushanbe was found to be 0.98 ± 0.01 during extreme dust events,

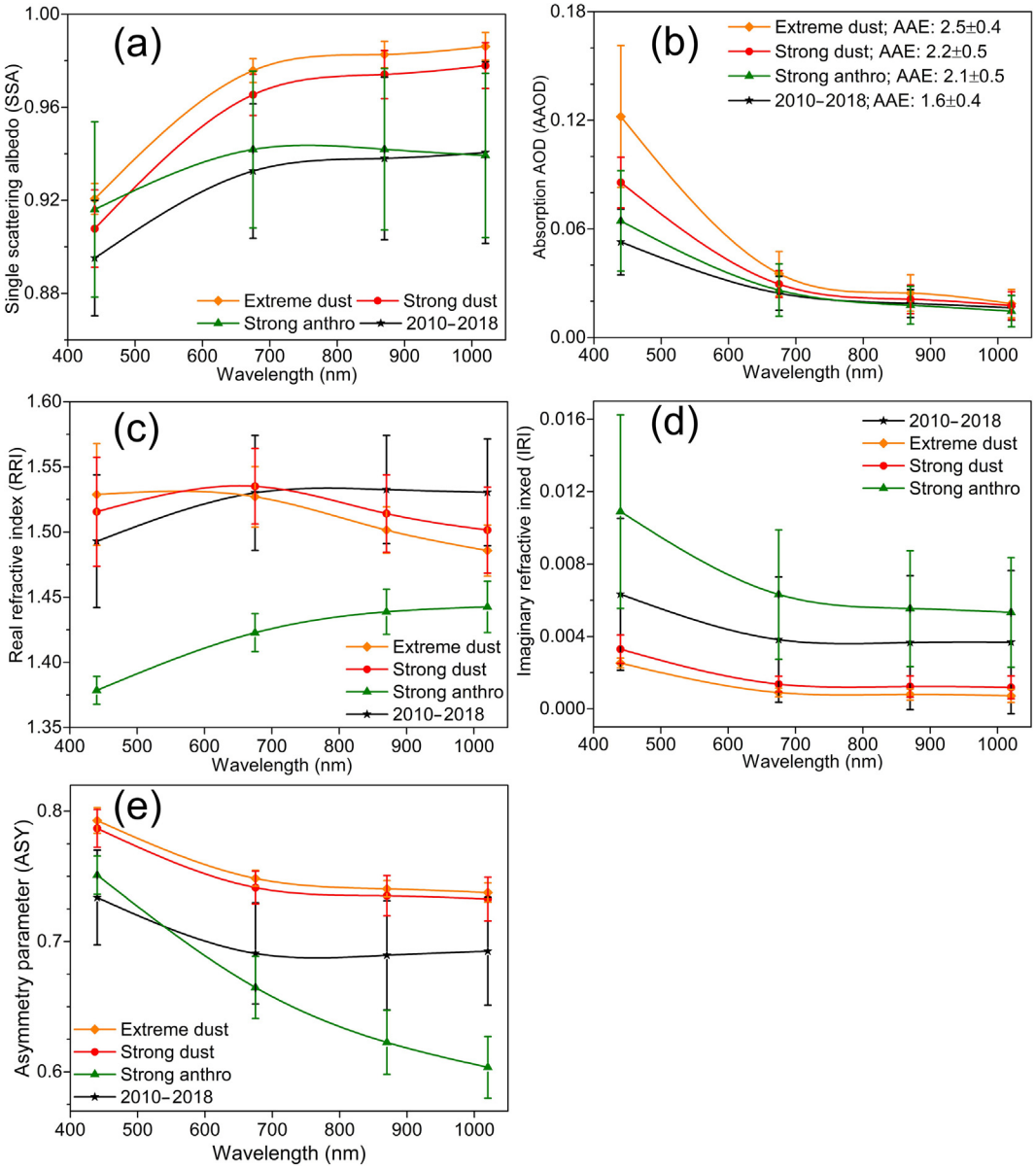

Fig. 5. (a) Single scattering albedo (SSA), (b) Absorption aerosol optical depth (AAOD), (c) Real part of aerosol refractive index (RRI), (d) Imaginary part of refractive index (IRI) and (e) Asymmetry parameter (ASY) during the observation period 2010–2018 and various aerosol events.

0.97 ± 0.01 for strong dust events, 0.94 ± 0.03 for strong anthropogenic aerosol events, and 0.93 ± 0.03 for 2010–2018 (all but events data), which are a clear indication of presence of abundant amount of scattering aerosols in atmosphere. Alam et al. (2014) reported similar values of SSA_{675} (0.98) during a dust event over Lahore, Pakistan. In the case of mineral dust particles, the spectral difference in SSA, i.e., ΔSSA as the difference between SSA_{1020} and SSA_{440}, is higher than 0.05 (Dubovik et al., 2002). In this study, average ΔSSA was found to be 0.066 for extreme dust events, 0.070 for strong dust events and 0.023 for strong anthropogenic aerosol events, clearly confirming the presence of mineral dust during the dust events. Similar values were reported during dust events over other nearby regions: 0.073–0.074 for Lahore, Pakistan (Alam et al., 2014), 0.051–0.073 (Prasad et al., 2007) and 0.073–0.104 (Kumar et al., 2015) for Kanpur, India. In addition, the values of AAE > 2.0 during the aerosol events (Fig. 5 b) also suggest a significant contribution from mineral dust aerosols (Russell et al., 2010).

The spectral variation of refractive index (*RI*), where the real part of *RI* (*RRI*) and the imaginary part of *RI* (*IRI*) are responsible for scattering and absorption, respectively (Sinyuk et al., 2003; Li et al., 2013) is presented in Fig. 5 (c and d). In Dushanbe, the extreme dust events had the average *RRI* (*IRI*) at 675 nm of 1.53 ± 0.02 (0.0009 ± 0.0002) while that for other two were, 1.54 ± 0.03 (0.0014 ± 0.0004) for strong dust events, and 1.42 ± 0.01 (0.0063 ± 0.0036) for strong anthropogenic aerosol events. *RRI* values at lower (higher) wavelengths were higher (lower) during extreme dust and strong dust events signifying the dominance of light-scattering mineral dust particles as supported by the higher values of SSA discussed earlier (Fig. 5a). Similar features were also observed over Lahore with the *RRI* (*IRI*) value at 675 nm of 1.52 (0.0009) (Alam et al., 2014), 1.56 ± 0.02 (0.0023 ± 0.0009) (Prasad and Singh, 2007), >1.5 (0.0008–0.003) (Tiwari et al., 2019), 1.54–1.60 (0.002–0.013) (Kumar et al., 2015) all over Kanpur in the IGP. The spectral characteristics of both *RRI* and *IRI* during the strong anthropogenic aerosol events

observed in Dushanbe were similar to those in the haze events observed over Lahore and Karachi in Pakistan (Iftikhar et al., 2018).

The Asymmetry Parameter (ASY), angular distribution of light scattered by aerosols with values ranging between −1 (completely backscattered) to +1 (completely forward scattered), is dependent upon particle size (inverse relation - smaller particles scatter more light to forward direction) and composition (Eck et al., 2005; Andrews et al., 2006). The average ASY exhibited a generally decreasing trend in the visible-infrared region (except for the events with strong anthropogenic aerosols which show a sharp decline) (Fig. 5e) confirming the dominance of coarse-mode aerosols. The mean ASY_{675} values during various cases were 0.75 ± 0.01 (extreme dust), 0.74 ± 0.01 (strong dust) and 0.66 ± 0.02 (strong anthropogenic). The ASY values during two types of dust events over Dushanbe were similar to the dust event observed in Lahore (Alam et al., 2014) and Kanpur (Tiwari et al., 2019). However, the abrupt decrease in ASY, during strong anthropogenic events, with the wavelength suggests the presence of fine aerosols in the atmosphere as indicated by the higher AE and FMF values mentioned in the earlier sections for this case. Similar characteristics have been reported in other studies too (Pandithurai et al., 2008; Iftikhar et al., 2018; Rupakheti et al., 2018).

3.4. Influence of aerosol events on radiative forcing and heating rates

The direct aerosol radiative forcing (ARF) at three levels, i.e., at the top of the atmosphere (ARF_{TOA}), at the bottom of the atmosphere (ARF_{BOA}), and in the atmosphere (ARF_{ATM}) for various aerosol events is presented in Fig. 6. The ARF_{TOA} is influenced by SSA (i.e., the composition of aerosols); ARF_{ATM} also depends on SSA whereas the ARF_{BOA} is influenced more by the change in aerosol loading (i.e., AOD) than change in SSA (Ramachandran and Rupakheti, 2020). The average ARF_{TOA}, ARF_{ATM} and ARF_{BOA} during 2010–2018 was −16 ± 8, 21 ± 11 and −37 ± 16 Wm^{-2}. They were −16.70, 33.40 and −50.10 Wm^{-2} respectively when all data (without separating into different events) during the whole period were considered (Rupakheti et al., 2020b). Negative value at TOA means atmospheric cooling due to light scattered back to the space whereas BOA also indicates cooling effect due to the reduction in solar radiation reaching the earth surface or simply the surface dimming effect (Kaskaoutis et al., 2013). During the extreme dust events, the mean values of ARF_{TOA}, ARF_{ATM} and ARF_{BOA} were −68 ± 19, 49 ± 21 and −117 ± 38 Wm^{-2}, whereas the respective ARF values for the strong dust events were −48 ± 12, 37 ± 15 and −85 ± 24 Wm^{-2}, and for the strong anthropogenic aerosol events they were −35 ± 7, 38 ± 17 and −73 ± 16 Wm^{-2}. The ARF_{TOA} and ARF_{BOA} were enhanced as compared with corresponding 2010–2018 values by a factor of ~2.3–4.3 and ~2.0–3.2, which clearly indicated that more solar energy was cut from reaching the earth's surface during the dust events than other days as more solar radiation was scattered by aerosols back to space (Tiwari et al., 2019). Furthermore, the positive values of ARF_{ATM}, which was higher by a factor of ~1.7–2.3 during the aerosol event days, clearly indicate that the dust and anthropogenic aerosols absorbed more solar radiation during the aerosol events and resulted in additional heating of the atmosphere by the aerosols.

Here, we would like to compare the results obtained over Dushanbe with other sites in nearby countries. Two dust events in 2013 over Zanjan, Iran resulted in ARF_{TOA}, ARF_{ATM} and ARF_{BOA} in between −40.23 and −11.9, 75.65 and 186.6, and −186 and −109.64 Wm^{-2} (Gharibzadeh et al., 2017). During a campaign conducted in 2019 in Kashi, China (about 200 km to the east of Tajikistan-China border), a dust event resulted in the cooling effect at TOA and BOA with an aerosol forcing up to −111 and −217 Wm^{-2}, respectively, and warming effect in ATM with a forcing of up to 121 Wm^{-2} (Li et al., 2020). Prasad et al. (2007) reported ARF_{TOA} of −13.5 Wm^{-2} and ARF_{BOA} of −57.5 Wm^{-2} during a dust outbreak over Kanpur in IGP. Other studies over Kanpur reported the ARF_{TOA}, ARF_{ATM} and ARF_{BOA} values during two intense dust storms in 2018 of −36.06 (-56.51), 124.40 (84.94) and −160.45 (-141.45) Wm^{-2}, respectively (Tiwari et al., 2019) and between −18 and −41, 37 and 75 and −66 and −101 Wm^{-2} during pre-monsoon dust storms that occurred in 2010 (Kumar et al., 2015). Similarly, dust events over Karachi and Lahore resulted in ARF_{TOA}, ARF_{ATM} and ARF_{BOA} to be −15 (−34), 34 (58) and −49 (−93) Wm^{-2}, respectively (Iftikhar et al., 2018). The dusty days in spring of

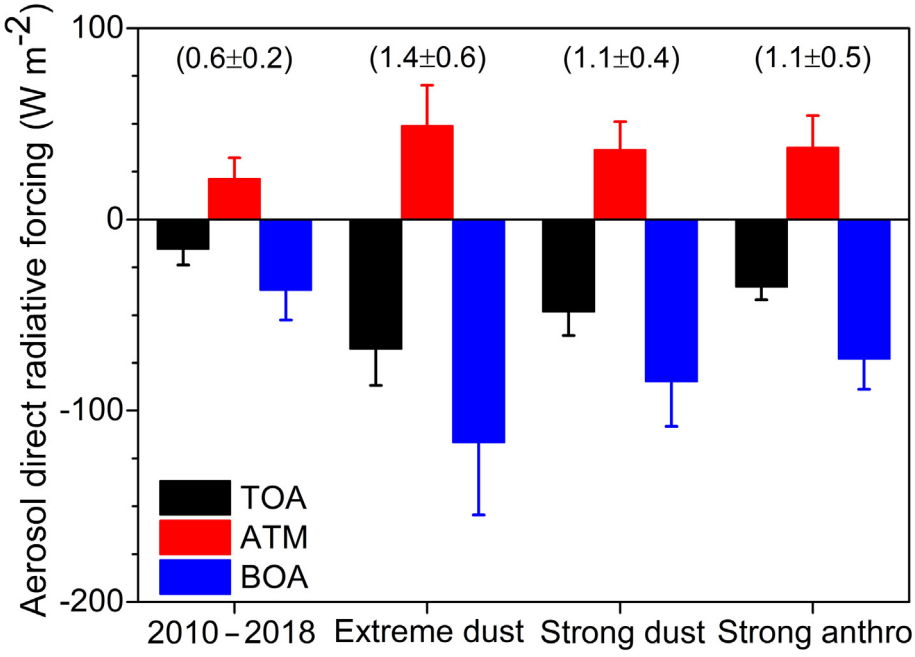

Fig. 6. Aerosol direct radiative forcing at the top of atmosphere (TOA), in the atmosphere (ATM) and bottom of atmosphere (BOA) for different scenarios. The value mentioned in parenthesis refers to the average heating rate in K day^{-1} (HR) ± one standard deviation.

2001–2014 in urban Beijing observed the ARF_{TOA} in between −121.80 and −72.95 W m^{-2} and RF_{BOA} in between −293.83 and −203.20 Wm^{-2} (Yu et al., 2016). The result suggested that the ARF_{ATM} during the onset of heavy aerosol events in Dushanbe is mostly lower compared to dust events observed in nearby regions (like IGP) known for heavy air pollution level.

The ARF_{BOA}/ARF_{TOA} ratio provides important information on the presence of light absorbing (>3.0) or scattering aerosols (<2.0) (Podgorny et al., 2000; Satheesh and Ramanathan, 2000). The mean ratio was 1.72 for the extreme dust events, 1.80 for the strong dust events, and 2.13 for the strong anthropogenic aerosol events over Dushanbe, which further strengthens the points presented earlier that light scattering aerosols dominated during the dust events.

Aerosol radiative forcing efficiency (ARFE), which is defined as the ARF per unit AOD (Wm^{-2} AOD^{-1}), can be utilized as an important parameter, beside SSA, to study the influence of absorbing and scattering properties of aerosols (García et al., 2008; Ramachandran and Rupakheti, 2020). During three types of heavy aerosol events in Dushanbe, the average ARFE at TOA, ATM and BOA were estimated as −46 ± 8, 34 ± 8 and −80 ± 13 Wm^{-2} AOD^{-1} during extreme dust events, −55 ± 9, 45 ± 15 and −100 ± 19 Wm^{-2} AOD^{-1} during strong dust events, and −53 ± 9, 44 ± 25 and −97 ± 20 Wm^{-2} AOD^{-1} during strong anthropogenic events, respectively. Similar values were reported recently during a dust event in Kashi, China in April 2019 where the ARFE was observed as −51, 55 and −99 Wm^{-2} AOD^{-1} at TOA, ATM and BOA (Li et al., 2020). Yu et al. (2016) reported the $ARFE_{TOA}$ in the range of −54.87 to −39.86 and $ARFE_{BOA}$ in the range from −147.23 to −120.51 W m^{-2} AOD^{-1} on the dust days during 2010–2014 spring season in Beijing. Kumar et al. (2015) reported, during dusty days over Kanpur in IGP in pre-monsoon season of 2010, the ARFE values of −19.86, 24.29 and −44.15 W m^{-2} AOD^{-1}, respectively. The ARFEs during the event days in Dushanbe were ~82%–98% (TOA), ~38%–50% (ATM) and ~55%–69% higher than the corresponding mean ARFE observed during 2010–2018 (non-event days), clearly demonstrating the influence of higher aerosol loading on radiative forcing during the pollution events.

Additionally, aerosol-induced heating rate (HR) was calculated to understand the influence of dust events in Dushanbe using the equation (Liou, 2002) provided below, Eq.(3):

$$\frac{\partial T}{\partial t} = \frac{g}{Cp} \times \frac{\Delta F_{ATM}}{\Delta P} \quad (3)$$

where, $\partial T/\partial t$ is the aerosol-induced atmospheric heating rate in Kelvin (K) day^{-1}, g is the acceleration due to the gravity (9.8 m s^{-2}), Cp is the specific heat capacity of the ambient air at constant pressure (1006 J kg^{-1} K^{-1}), ΔF_{ATM} is the ARF_{ATM} (in Wm^{-2}), and ΔP (hPa) is the difference in atmospheric pressure between surface and the height of 3 km (~30,000 Pa) over the measurement site. Three km is considered as the majority of atmospheric aerosols are present within 3 km from the surface.

Onset of heavy dust or haze events has proven to influence the aerosol-induced heating rates (Srivastava et al., 2014; Tiwari et al., 2019). There was an enhancement in the HR during all three types of events in Dushanbe: ~2.3 times higher during extreme dust events, and ~1.8 times during both strong dust events and strong anthropogenic events than the average HR during 2010–2018 (Fig. 6). The heating rates were found in the range of 0.8–2.7 (mean ± SD: 1.4 ± 0.6) K day^{-1} during the extreme dust events, 0.4–1.9 (1.1 ± 0.4) K day^{-1} during the strong dust events, and 0.5–1.6 (1.1 ± 0.5) K day^{-1} during the strong anthropogenic aerosol events. The *HR* values higher than in our study have been reported during south Asian dust storm observed over Delhi (2.0 K day^{-1}) and Jodhpur (1.9 K day^{-1}) (Srivastava et al., 2014). During the dust episodes, the *HR* values reported for various sites in Asia were 0.78–2.70 K day^{-1} over Kanpur in India (Kumar et al., 2015; Tiwari et al., 2019), 0.7–1.4 over Karachi and 1.3–2.2 K day^{-1} over Lahore in Pakistan (Iftikhar et al., 2018), 2.44–3.76 K day^{-1} over Beijing in China (Yu et al., 2016), 0.89–2.16 K day^{-1} over Zanjan in Iran (Gharibzadeh et al., 2017). Rupakheti et al. (2020a) reported the onset of heavy haze events due mostly to pollution aerosols over the Lumbini (northern edge of central IGP) in Nepal resulted in the HR of ~ 5–7 K day^{-1}.

3.5. Air mass origin and transport during pollution events

The pathways of air mass transport before the onset of all types of aerosol events discussed in this study is presented in Fig. 7. The history of trajectories of air masses that arrived at the height of 500 m (above the ground) at 00:00 local time of the event days above Dushanbe was tracked for 5 days. Regarding the extreme events (Fig. 7 a, b, c), the air mass during the extreme dust events – 2, 7, 8, 9 and 13 were of broad regional, i.e., the air masses were transported over long-range in the region. Unlike the fine-mode dust particles, the coarse mode dust particles are unlikely to get transported over long distance because they get settled to the ground within short distance due to gravity. For the strong dust events (Fig. 7 d, e, f) and strong anthropogenic aerosol events (Fig. 7 g) too, most of the air masses were of local or regional origin. We also investigated the origin/transport of air mass for 24 h before the onset of three events with highest aerosol loading under each category (Supplementary Data, Fig. S4). In the case of the top three extreme dust events, we found that the air mass either originated in Tajikistan and then passed over Uzbekistan before reaching Dushanbe or were originated in Tajikistan itself and travelled to Dushanbe carrying dust from those regions. It was the similar scenario during strong dust events but with some contribution of air mass originated over Turkmenistan. We observed an interesting pattern of air mass for the day with second highest AOD during the strong dust event (Oct 11th 2015) when we tracked the route for 96 h (not shown here). The routes of the air mass arriving at 1000 m and 1500 m originated near Dushanbe, travelled westward all the way to the central Turkmenistan and returned back to Dushanbe. However, the air mass at 500 m was originated over Afghanistan that later on reached Turkmenistan and followed the same path as the other air masses to arrive at Dushanbe. During the top three strong anthropogenic events, the air masses at lower heights (500 and 1500 m) were from Tajikistan itself. The route of air mass at the lowest height (500 m) was very short which signifies very stagnant air resulting in pollution build up during the strong anthropogenic events. Interestingly, most of these air masses travelled very close to the ground (carrying along the local emissions along their paths) and rose to their respective heights from 5 to 6 h before the occurrence of events. However, during some events (extreme dust (Supplementary Data, Fig. S4a) or Strong dust (Supplementary Data, Fig. S4b)), the air mass descended from much higher altitude. To sum up, both local and regional (normally crossing over neighbouring countries) air masses were responsible for the occurrence of dust and anthropogenic air pollution events over Dushanbe.

3.6. Role of synoptic circulations in modulating the aerosol properties

The distinctly different aerosol types (UI/BB and dust) and characteristics (AOD, AE, SSA, AAOD, VSD etc.) and back trajectories of the air masses that arrived at Dushanbe during the dust events and the anthropogenic aerosol events suggest that development and evolution of different synoptic-scale meteorological circulation influenced the transport of different aerosols from different source regions into the Dushanbe atmosphere. In case of extreme dust events, a slow eastward moving synoptic system with a well-developed high-pressure system (located over the Kazakhstan-

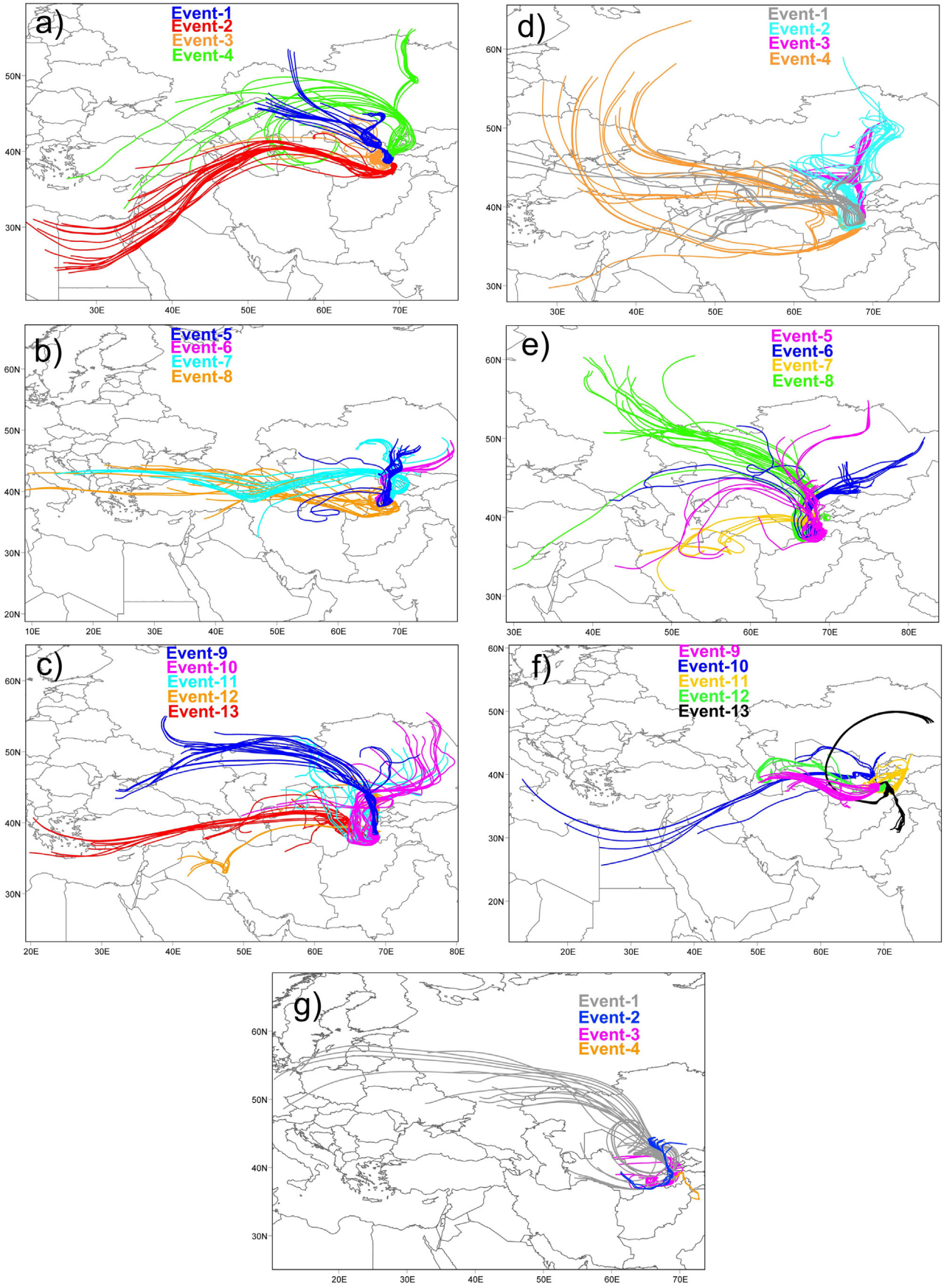

Fig. 7. Five-day long back trajectories of air masses arriving Dushanbe site at 00:00 local time of the event days. (a, b, c) show air mass back trajectories for the thirteen extreme dust events, (d, e, f) for the thirteen strong dust events, and (g) for the four extreme anthropogenic events.

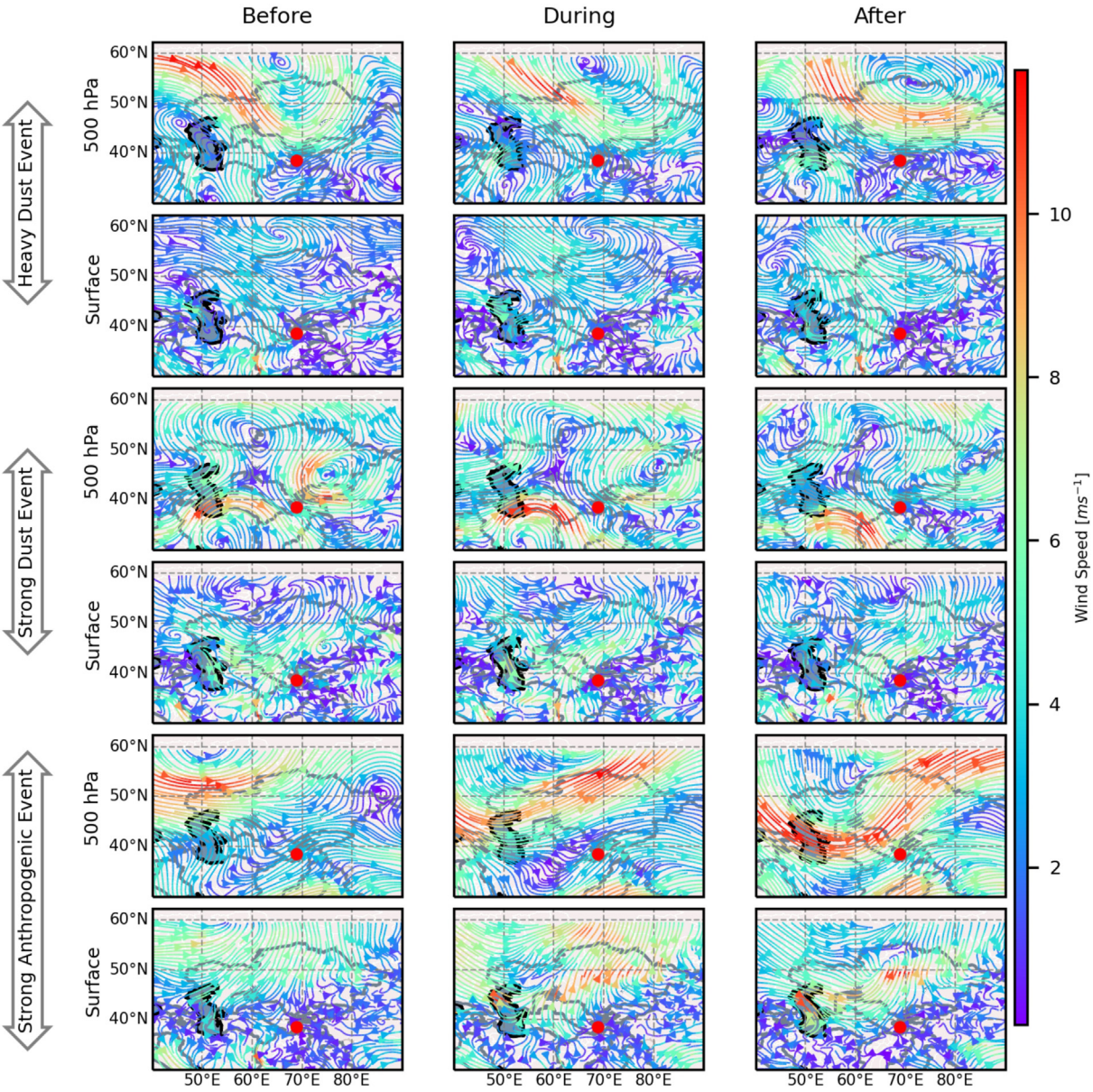

Fig. 8. Synoptic circulation at 500 hPa and surface before, during and after the events with highest aerosol loading under each category.

Russia border) to the north of Dushanbe and a relatively poorly developed low-pressure system (located over area south of the Caspian Sea) to the south of Dushanbe (e.g., extreme dust event on 15th July 2016, Fig. 8). This slow moving synoptic system created a dust storm spreading over thousands of kilometers in the region (Supplementary Data, Fig. S1). A narrow channel of strong northwesterly winds at both 500 mb and surface over southern Kazakhstan, Uzbekistan transported dust from the dry lands in southern Kazakhstan, Uzbekistan and Turkmenistan into the inter-mountain basin to the west of the Pamir mountain range. This, combined with calm wind conditions (as observed at the Dushanbe International Airport), led to dusty-hazy condition over the basin (see air mass back trajectories in Fig. 7 and satellite image in Supplementary Data, Fig. S1). The extent of dust loading over Dushanbe during dust events depend on the strength and location of the high-pressure and low-pressure systems and trajectories of the air masses before arriving to the Dushanbe site. Location of high-pressure system further north resulted in less dust loading over Dushanbe. Likewise, air masses that arrived directly at Dushanbe after passing over dry regions over southern Kazakhstan, Uzbekistan and Turkmenistan resulted in higher loading of dust over Dushanbe. In case of anthropogenic aerosol events, the synoptic system was less- or un-organized than during the dust events, with south-westerly or westerly synoptic winds at 500 mb and the surface (Fig. 7g, Fig. 8) and calm local winds over Dushanbe created conditions conducive to accumulation of anthropogenic emissions over the basin.

4. Conclusion

This study was conducted with an aim to investigate the modification in aerosol physical, optical and radiative properties during high dust and anthropogenic aerosol events over Dushanbe, the capital city of Tajikistan in Central Asia. Data acquired with a sun-photometer installed under the NASA AERONET over an 8-year period (2010–2018) was utilized. The AOD during three cases with extreme dust events, strong dust events and strong anthropogenic aerosol events were ~6.6, 3.5 and 3 times higher than average AOD

during 2010–2018 (without those events). Presence of dust aerosols resulted in very low AE and FMF especially during first two types of events, however much larger values during strong anthropogenic events. The analysis of various aerosol parameters confirmed the aerosol types during the events, for instance VSD, SSA, ASY and RI all confirmed the dominant presence of coarse-mode aerosols during the extreme dust events and the strong dust events but of fine-mode aerosols during the strong anthropogenic aerosol events. These heavy aerosol events resulted in cooling effects, measured in terms of aerosol radiative forcing (ARF), a factor of 2.2–4.3 times higher at the top of the atmosphere (TOA) and 2–3.2 at the bottom of the atmosphere (BOA) and warming effect with ARF 1.8–2.3 times higher in the atmosphere (ATM) as compared with the 2010–2018 case (all but events data). Increase in aerosol loading enhanced the aerosol-induced warming of the atmosphere with a heating rate of 0.8–2.7 K day^{-1} during the extreme dust, 0.4–1.9 K day^{-1} during the strong dust, and 0.5–1.6 K day^{-1} during the strong anthropogenic aerosol events, clearly suggesting that the dust and/or anthropogenic aerosols can exert a significant change in the radiative balance of the atmosphere over Central Asia, and the aerosol-induced heating rate of the atmosphere (ca. 0.5–2.0 K day^{-1}) is quite high. As evidenced by air-mass back trajectories, mostly the air mass originated at local and regional scale 'fuel-up' the occurrence of high aerosol events over Dushanbe. Our study suggest that the dust and anthropogenic aerosols, in particular the extreme events as they can exert disproportionally high radiative impacts, over Central Asia need to be considered carefully in understanding and estimating the radiative and other impacts of aerosols in the Central Asia and downwind regions like Tian Shan, Himalayas and Tibetan Plateau.

Data availability

Publicly available datasets have been used in this study. The columnar aerosol dataset were retrieved from the AERONET website (https://aeronet.gsfc.nasa.gov/). Sources of other datasets used in this study have been mentioned in the manuscript.

Author contributions

D. Rupakheti, M. Rupakheti and S. Kang developed the ideas and designed the study. S. F. Abdullaev maintained the site and collected the data. X. Yin and J. Hofer provided constructive comments and M. Rai and Y. Hu helped with the figure preparation. D. Rupakheti wrote the manuscript under the supervision of S. Kang and with substantial contributions from all authors.

Declaration of Competing Interest

The authors declare that they have no known competing financial interests or personal relationships that could have appeared to influence the work reported in this paper.

Acknowledgements

This study was supported by the Strategic Priority Research Program of Chinese Academy of Sciences, Pan-Third Pole Environment Study for a Green Silk Road (Pan-TPE) (XDA20040501), the National Natural Science Foundation of China (41907328, 41630754) and State Key Laboratory of Cryospheric Science (SKLCS-ZZ-2020). Dipesh Rupakheti acknowledges CAS-President's International Fellowship Initiative (PIFI, Grant no. 2019PC0076). Maheswar Rupakheti acknowledges the support provided by the Institute for Advanced Sustainability Studies (IASS), which is funded by the German Federal Ministry for Education and Research (BMBF) and the Brandenburg Ministry for Science, Research and Culture (MWFK). Sabur F. Abdullaev acknowledges the International Science and Technology Center (ISTC) Projects (T-1688 and T-2076). All authors are grateful to Brent Holben (NASA GSFC, USA) for the establishment of the AERONET site, and Prof. Phillipe Goloub and staffs for their efforts for the annual calibration of the sunphotometer.

Appendix A. Supplementary data

Supplementary data to this article can be found online at https://doi.org/10.1016/j.gsf.2021.101251.

References

Abdullaev, S.F., Maslov, V.A., Nazarov, B.I., Minikulov, N.K., Djuraev, A.M., 2019. Variations of aerosol optical thickness, water vapor and Ångström parameter over the semi-arid zone of Tajikistan, in: E3S Web of Conferences. pp. 1–4. https://doi.org/10.1051/e3sconf/20199903004.

Abdullaev, S.F., Maslov, V.A., Nazarov, B.I., Salikhov, T.K., 2014. Variations in parameters of aerosol optical thickness in Dushanbe. Izv. Atmos. Ocean Phys. 50, 431–434. https://doi.org/10.1134/S0001433814030025.

Abdullaev, S.F., Sokolik, I.N., 2019. Main characteristics of dust storm sand their radiative impacts: with a Focuson Tajikistan. J. Atmos. Sci. Res. 2, 1–21. https://doi.org/10.30564/jasr.v2i2.352.

Alam, K., Trautmann, T., Blaschke, T., Subhan, F., 2014. Changes in aerosol optical properties due to dust storms in the Middle East and Southwest Asia. Remote Sens. Environ. 143, 216–227. https://doi.org/10.1016/j.rse.2013.12.021.

Andrews, E., Sheridan, P.J., Fiebig, M., McComiskey, A., Ogren, J.A., Arnott, P., Covert, D., Elleman, R., Gasparini, R., Collins, D., Jonsson, H., Schmid, B., Wang, J., 2006. Comparison of methods for deriving aerosol asymmetry parameter. J. Geophys. Res. 111, 1–16. https://doi.org/10.1029/2004JD005734.

Bergstrom, R.W., Pilewskie, P., Russell, P.B., Redemann, J., Bond, T.C., Quinn, P.K., Sierau, B., 2007. Spectral absorption properties of atmospheric aerosols. Atmos. Chem. Phys. 7, 5937–5943. https://doi.org/10.5194/acp-7-5937-2007.

Draxler, R.R., Hess, G.D., 1998. An overview of the HYSPLIT_4 modelling system for trajectories, dispersion, and deposition. Aust. Meteorol. Mag. 47, 295–308.

Dubovik, O., King, M.D., 2000. A flexible inversion algorithm for retrieval of aerosol optical properties from Sun and sky radiance measurements. J. Geophys. Res. 105, 20673–20696. https://doi.org/10.1029/2000JD900282.

Dubovik, O., Kaufman, Y.J., King, M.D., Eck, T.F., Smirnov, A., Tanré, D., Holben, B., Slutsker, I., 2002. Variability of absorption and optical properties of key aerosol types observed in worldwide locations. J. Atmos. Sci. 59, 590–608. https://doi.org/10.1175/1520-0469(2002)059<0590:voaaop>2.0.co;2.

Eck, T.F., Holben, B.N., Dubovik, O., Smirnov, A., Goloub, P., Chen, H.B., Chatenet, B., Gomes, L., Zhang, X.-Y., Tsay, S.-C., Ji, Q., Giles, D., Slutsker, I., 2005. Columnar aerosol optical properties at AERONET sites in central eastern Asia and aerosol transport to the tropical mid-Pacific. J. Geophys. Res. 110, n/a–n/a. https://doi.org/10.1029/2004JD005274.

García, O.E., Díez, A.M., Expósito, F.J., Díaz, J.P., Dubovik, O., Dubuisson, P., Roger, J.C., Eck, T.F., Sinyuk, A., Derimian, Y., Dutton, E.G., Schafer, J.S., Holben, B., García, C. A., 2008. Validation of AERONET estimates of atmospheric solar fluxes and aerosol radiative forcing by ground-based broadband measurements. J. Geophys. Res. 113, 1–16. https://doi.org/10.1029/2008JD010211.

Gharibzadeh, M., Alam, K., Bidokhti, A.A., Abedini, Y., Masoumi, A., 2017. Radiative effects and optical properties of aerosol during two dust events in 2013 over Zanjan, Iran. Aerosol Air Qual. Res. 17, 888–898. https://doi.org/10.4209/aaqr.2016.04.0161.

Giles, D.M., Holben, B.N., Eck, T.F., Sinyuk, A., Smirnov, A., Slutsker, I., Dickerson, R.R., Thompson, A.M., Schafer, J.S., 2012. An analysis of AERONET aerosol absorption properties and classifications representative of aerosol source regions. J. Geophys. Res. 117, n/a–n/a. https://doi.org/10.1029/2012JD018127.

Giles, D.M., Sinyuk, A., Sorokin, M.S., Schafer, J.S., Smirnov, A., Slutsker, I., Eck, T.F., Holben, B.N., Lewis, J., Campbell, J., Welton, E.J., Korkin, S., Lyapustin, A., 2019. Advancements in the Aerosol Robotic Network (AERONET) Version 3 Database – Automated Near Real-Time Quality Control Algorithm with Improved Cloud Screening for Sun Photometer Aerosol Optical Depth (AOD) Measurements. Atmos. Meas. Tech. 12, 169–209. https://doi.org/10.5194/amt-12-169-2019.

Ginoux, P., Prospero, J., Torres, O., Chin, M., 2004. Long-term simulation of global dust distribution with the GOCART model: correlation with North Atlantic Oscillation. Environ. Model. Softw. 19, 113–128. https://doi.org/10.1016/S1364-8152(03)00114-2.

Gkikas, A., Basart, S., Hatzianastassiou, N., Marinou, E., Amiridis, V., Kazadzis, S., Pey, J., Querol, X., Jorba, O., Gassó, S., Baldasano, J.M., 2016. Mediterranean intense desert dust outbreaks and their vertical structure based on remote sensing data. Atmos. Chem. Phys. 16, 8609–8642. https://doi.org/10.5194/acp-16-8609-2016.

Gkikas, A., Hatzianastassiou, N., Mihalopoulos, N., 2009. Aerosol events in the broader Mediterranean basin based on 7-year (2000–2007) MODIS C005 data. Ann. Geophys. 27, 3509–3522. https://doi.org/10.5194/angeo-27-3509-2009.

Gkikas, A., Hatzianastassiou, N., Mihalopoulos, N., Katsoulis, V., Kazadzis, S., Pey, J., Querol, X., Torres, O., 2013. The regime of intense desert dust episodes in the Mediterranean based on contemporary satellite observations and ground measurements. Atmos. Chem. Phys. 13, 12135–12154. https://doi.org/10.5194/acp-13-12135-2013.

Hersbach, H., Bell, B., Berrisford, P., Hirahara, S., Horányi, A., Muñoz-Sabater, J., Nicolas, J., Peubey, C., Radu, R., Schepers, D., Simmons, A., Soci, C., Abdalla, S., Abellan, X., Balsamo, G., Bechtold, P., Biavati, G., Bidlot, J., Bonavita, M., Chiara, G., Dahlgren, P., Dee, D., Diamantakis, M., Dragani, R., Flemming, J., Forbes, R., Fuentes, M., Geer, A., Haimberger, L., Healy, S., Hogan, R.J., Hólm, E., Janisková, M., Keeley, S., Laloyaux, P., Lopez, P., Lupu, C., Radnoti, G., Rosnay, P., Rozum, I., Vamborg, F., Villaume, S., Thépaut, J.-N., 2020. The ERA5 global reanalysis. Q. J. R. Meteorol. Soc. 146, 1999–2049. https://doi.org/10.1002/qj.v146.73010.1002/qj.3803.

Hofer, J., Althausen, D., Abdullaev, S.F., Makhmudov, A.N., Nazarov, B.I., Schettler, G., Engelmann, R., Baars, H., Fomba, K.W., Müller, K., Heinold, B., Kandler, K., Ansmann, A., 2017. Long-term profiling of mineral dust and pollution aerosol with multiwavelength polarization Raman lidar at the Central Asian site of Dushanbe, Tajikistan: Case studies. Atmos. Chem. Phys. 17, 14559–14577. https://doi.org/10.5194/acp-17-14559-2017.

Hofer, J., Ansmann, A., Althausen, D., Engelmann, R., Baars, H., Abdullaev, S.F., Makhmudov, A.N., 2020. Long-term profiling of aerosol light extinction, particle mass, cloud condensation nuclei, and ice-nucleating particle concentration over Dushanbe, Tajikistan, in Central Asia. Atmos. Chem. Phys. 20, 4695–4711. https://doi.org/10.5194/acp-20-4695-2020.

Holben, B.N., Eck, T.F., Slutsker, I., Tanré, D., Buis, J.P., Setzer, A., Vermote, E., Reagan, J.A., Kaufman, Y.J., Nakajima, T., Lavenu, F., Jankowiak, I., Smirnov, A., 1998. AERONET - A federated instrument network and data archive for aerosol characterization. Remote Sens. Environ. 66, 1–16. https://doi.org/10.1016/S0034-4257(98)00031-5.

Holben, B.N., Tanré, D., Smirnov, A., Eck, T.F., Slutsker, I., Abuhassan, N., Newcomb, W.W., Schafer, J.S., Chatenet, B., Lavenu, F., Kaufman, Y.J., Vande Castle, J., Setzer, A., Markham, B., Clark, D., Frouin, R., Halthore, R., Karneli, A., O'Neill, N.T., Pietras, C., Pinker, R.T., Voss, K., Zibordi, G., Tanre, D., Smirnov, A., Eck, T.F., Slutsker, I., Abuhassan, N., Newcomb, W.W., Schafer, J.S., Chatenet, B., Lavenu, F., Kaufman, Y.J., Castle, J.V., Setzer, A., Markham, B., Clark, D., Frouin, R., Halthore, R., Karneli, A., O'Neill, N.T., Pietras, C., Pinker, R.T., Voss, K., Zibordi, G., 2001. An emerging ground-based aerosol climatology: aerosol optical depth from AERONET. J. Geophys. Res. 106, 12067–12097. https://doi.org/10.1029/2001JD900014.

Huang, J., Wang, T., Wang, W., Li, Z., Yan, H., 2014. Climate effects of dust aerosols over East Asian arid and semiarid regions. J. Geophys. Res. Atmos. 119, 11398–11416. https://doi.org/10.1002/2014JD021796.

Huang, J., Zhang, C., Prospero, J.M., 2010. African dust outbreaks: a satellite perspective of temporal and spatial variability over the tropical Atlantic Ocean. J. Geophys. Res. 115, 1–20. https://doi.org/10.1029/2009JD012516.

Iftikhar, M., Alam, K., Sorooshian, A., Syed, W.A., Bibi, S., Bibi, H., 2018. Contrasting aerosol optical and radiative properties between dust and urban haze episodes in megacities of Pakistan. Atmos. Environ. 173, 157–172. https://doi.org/10.1016/j.atmosenv.2017.11.011.

Immerzeel, W.W., van Beek, L.P.H., Bierkens, M.F.P., 2010. Climate change will affect the asian water towers. Science 328, 1382–1385. https://doi.org/10.1126/science:1183188.

IPCC, 2013. Climate Change 2013: The Physical Science Basis. Cambridge University Press, Cambridge, p. 1535.

Issanova, G., Abuduwaili, J., 2017. Aeolian Processes as Dust Storms in the Deserts of Central Asia and Kazakhstan. Springer Singapore, Singapore.

Kang, S., Zhang, Q., Qian, Y., Ji, Z., Li, C., Cong, Z., Zhang, Y., Guo, J., Du, W., Huang, J., You, Q., Panday, A.K., Rupakheti, M., Chen, D., Gustafsson, Ö., Thiemens, M.H., Qin, D., 2019. Linking atmospheric pollution to cryospheric change in the Third Pole region: current progress and future prospects. Natl. Sci. Rev. 6, 796–809. https://doi.org/10.1093/nsr/nwz031.

Kaskaoutis, D.G., Sinha, P.R., Vinoj, V., Kosmopoulos, P.G., Tripathi, S.N., Misra, A., Sharma, M., Singh, R.P., 2013. Aerosol properties and radiative forcing over Kanpur during severe aerosol loading conditions. Atmos. Environ. 79, 7–19. https://doi.org/10.1016/j.atmosenv.2013.06.020.

Kaskaoutis, D.G., Kambezidis, H.D., Hatzianastassiou, N., Kosmopoulos, P.G., Badarinath, K.V.S., 2007. Aerosol climatology: on the discrimination of aerosol types over four AERONET sites. Atmos. Chem. Phys. Discuss. 7, 6357–6411. https://doi. org/10.5194/acpd-7-6357-2007.

Kaspari, S., Painter, T.H., Gysel, M., Skiles, S.M., Schwikowski, M., 2014. Seasonal and elevational variations of black carbon and dust in snow and ice in the Solu-Khumbu, Nepal and estimated radiative forcings. Atmos. Chem. Phys. 14, 8089–8103. https://doi.org/10.5194/acp-14-8089-2014.

Kumar, K.R., Boiyo, R., Madina, A., Kang, N., 2018. A 13-year climatological study on the variations of aerosol and cloud properties over Kazakhstan from remotely sensed satellite observations. J. Atmos. Solar-Terrestrial Phys. 179, 55–68. https://doi.org/10.1016/j.jastp.2018.06.014.

Kumar, S., Kumar, S., Kaskaoutis, D.G., Singh, R.P., Singh, R.K., Mishra, A.K., Srivastava, M.K., Singh, A.K., 2015. Meteorological, atmospheric and climatic perturbations during major dust storms over Indo-Gangetic Basin. Aeolian Res. 17, 15–31. https://doi.org/10.1016/j.aeolia.2015.01.006.

Li, L., Li, Z., Chang, W., Ou, Y., Goloub, P., Li, C., Li, K., Hu, Q., Wang, J., Wendisch, M., 2020. Aerosol solar radiative forcing near the Taklimakan Desert based on radiative transfer and regional meteorological simulations during the Dust Aerosol Observation-Kashi campaign. Atmos. Chem. Phys. 20, 10845–10864. https://doi.org/10.5194/acp-20-10845-2020.

Li, Z., Gu, X., Wang, L., Li, D., Xie, Y., Li, K., Dubovik, O., Schuster, G., Goloub, P., Zhang, Y., Li, L., Ma, Y., Xu, H., 2013. Aerosol physical and chemical properties retrieved from ground-based remote sensing measurements during heavy haze days in Beijing winter. Atmos. Chem. Phys. 13, 10171–10183. https://doi.org/10.5194/acp-13-10171-2013.

Liou, K.N., 2002. An Introduction to Atmospheric Radiation. Academic Press, New York.

Liu, J., Ding, J., Li, L., Li, X., Zhang, Z., Ran, S.i., Ge, X., Zhang, J., Wang, J., 2020. Characteristics of aerosol optical depth over land types in central Asia. Sci. Total Environ. 727, 138676. https://doi.org/10.1016/j.scitotenv.2020.138676.

Liu, Y., Zhu, Q., Wang, R., Xiao, K., Cha, P., 2019. Distribution, source and transport of the aerosols over Central Asia. Atmos. Environ. 210, 120–131. https://doi.org/10.1016/j.atmosenv.2019.04.052.

Mahowald, N.M., Engelstaedter, S., Luo, C., Sealy, A., Artaxo, P., Benitez-Nelson, C., Bonnet, S., Chen, Y., Chuang, P.Y., Cohen, D.D., Dulac, F., Herut, B., Johansen, A.M., Kubilay, N., Losno, R., Maenhaut, W., Paytan, A., Prospero, J.M., Shank, L.M., Siefert, R.L., 2009. Atmospheric iron deposition: global distribution, variability, and human perturbations. Ann. Rev. Mar. Sci. 1, 245–278. https://doi.org/10.1146/annurev.marine.010908.163727.

Middleton, N.J., 2017. Desert dust hazards: a global review. Aeolian Res. 24, 53–63. https://doi.org/10.1016/j.aeolia.2016.12.001.

Miller, R.L., Tegen, I., Perlwitz, J., 2004. Surface radiative forcing by soil dust aerosols and the hydrologic cycle. J. Geophys. Res. 109, n/a–n/a. https://doi.org/10.1029/2003JD004085.

Muhs, D.R., Budahn, J.R., Prospero, J.M., Carey, S.N., 2007. Geochemical evidence for African dust inputs to soils of western Atlantic islands: Barbados, the Bahamas, and Florida. J. Geophys. Res. 112, 1–26. https://doi.org/10.1029/2005JF000445.

Pandithurai, G., Dipu, S., Dani, K.K., Tiwari, S., Bisht, D.S., Devara, P.C.S., Pinker, R.T., 2008. Aerosol radiative forcing during dust events over New Delhi, India. J. Geophys. Res. 113, 1–13. https://doi.org/10.1029/2008JD009804.

Penner, J.E., 2001. Aerosols, their Direct and Indirect Effects, in: Climate Change 2001: The Scientific Basis, Contribution of Working Group I to IPCC. Cambridge Univ. Press, Cambridge, U. K., and New York, pp. 291–336.

Podgorny, I.A., Conant, W., Ramanathan, V., Satheesh, S.K., 2000. Aerosol modulation of atmospheric and surface solar heating over the tropical Indian Ocean. Tellus Ser. B Chem. Phys. Meteorol. 52, 947–958. https://doi.org/10.3402/tellusb:v52i3.17077.

Prasad, A.K., Singh, R.P., 2007. Comparison of MISR-MODIS aerosol optical depth over the Indo-Gangetic basin during the winter and summer seasons (2000–2005). Remote Sens. Environ. 107, 109–119. https://doi.org/10.1016/j.rse.2006.09.026.

Prasad, A., Singh, S., Chauhan, S., Srivastava, M., Singh, R., Singh, R., 2007. Aerosol radiative forcing over the Indo-Gangetic plains during major dust storms. Atmos. Environ. 41, 6289–6301. https://doi.org/10.1016/j.atmosenv.2007.03.060.

Prospero, J.M., Landing, W.M., Schulz, M., 2010. African dust deposition to Florida: temporal and spatial variability and comparisons to models. J. Geophys. Res. 115, 1–19. https://doi.org/10.1029/2009JD012773.

Ramachandran, S., Rupakheti, M., 2020. Inter-annual and seasonal variations in columnar aerosol characteristics and radiative effects over the Pokhara Valley in the Himalayan foothills – Composition, radiative forcing, and atmospheric heating. Environ. Pollut. 264, 114799. https://doi.org/10.1016/j.envpol.2020.114799.

Rupakheti, D., Kang, S., Bilal, M., Gong, J., Xia, X., Cong, Z., 2019a. Aerosol optical depth climatology over Central Asian countries based on Aqua-MODIS Collection 6.1 data: Aerosol variations and sources. Atmos. Environ. 207, 205–214. https://doi.org/10.1016/j.atmosenv.2019.03.020.

Rupakheti, D., Kang, S., Rupakheti, M., 2020a. Two heavy haze events over Lumbini in southern Nepal: enhanced aerosol radiative forcing and heating rates. Atmos. Environ. 236, 1–13. https://doi.org/10.1016/j.atmosenv.2020.117658.

Rupakheti, D., Kang, S., Rupakheti, M., Cong, Z., Panday, A.K., Holben, B.N., 2019b. Identification of absorbing aerosol types at a site in the northern edge of Indo-Gangetic Plain and a polluted valley in the foothills of the central Himalayas. Atmos. Res. 223, 15–23. https://doi.org/10.1016/j.atmosres.2019.03.003.

Rupakheti, D., Kang, S., Rupakheti, M., Cong, Z., Tripathee, L., Panday, A.K., Holben, B. N., 2018. Observation of optical properties and sources of aerosols at Buddha's birthplace, Lumbini, Nepal: environmental implications. Environ. Sci. Pollut. Res. 25, 14868–14881. https://doi.org/10.1007/s11356-018-1713-z.

Rupakheti, D., Rupakheti, M., Abdullaev, S.F., Yin, X., Kang, S., 2020b. Columnar aerosol properties and radiative effects over Dushanbe, Tajikistan in Central Asia. Environ. Pollut. 265, 1–12. https://doi.org/10.1016/j.envpol.2020.114872.

Russell, P.B., Bergstrom, R.W., Shinozuka, Y., Clarke, A.D., Decarlo, P.F., Jimenez, J.L., Livingston, J.M., Redemann, J., Dubovik, O., Strawa, A., 2010. Absorption Angstrom Exponent in AERONET and related data as an indicator of aerosol composition. Atmos. Chem. Phys. 10, 1155–1169. https://doi.org/10.5194/acp-10-1155-2010.

Russell, P.B., Kacenelenbogen, M., Livingston, J.M., Hasekamp, O.P., Burton, S.P., Schuster, G.L., Johnson, M.S., Knobelspiesse, K.D., Redemann, J., Ramachandran, S., Holben, B., Mahen Konwar1, S. K. Das1, S. M. Deshpande1, K. Chakravarty1, and B.N.G., 2014. A multiparameter aerosol classification method and its application to retrievals from spaceborne polarimetry. J. Geophys. Res. Atmos. 119, 9838–9863. https://doi.org/10.1002/2013JD021411.

Satheesh, S.K., Ramanathan, V., 2000. Large differences in tropical aerosol forcing at the top of the atmosphere and Earth ' s surface. Nature 405, 60–63.

Seinfeld, J.H., Pandis, S.N., 2016. Atmospheric Chemistry and Physics: From Air Pollution to Climate Change. John Wiley & Sons, Hoboken.
Sinyuk, A., Torres, O., Dubovik, O., 2003. Combined use of satellite and surface observations to infer the imaginary part of refractive index of Saharan dust. Geophys. Res. Lett. 30, 3–6. https://doi.org/10.1029/2002GL016189.
Smirnov, A., Holben, B.N., Eck, T.F., Dubovik, O., Slutsker, I., 2000. Cloud-screening and quality control algorithms for the AERONET database. Remote Sens. Environ. 73, 337–349. https://doi.org/10.1016/S0034-4257(00)00109-7.
Srivastava, A.K., Soni, V.K., Singh, S., Kanawade, V.P., Singh, N., Tiwari, S., Attri, S.D., 2014. An early South Asian dust storm during March 2012 and its impacts on Indian Himalayan foothills: a case study. Sci. Total Environ. 493, 526–534. https://doi.org/10.1016/j.scitotenv.2014.06.024.
Stein, A.F., Draxler, R.R., Rolph, G.D., Stunder, B.J.B., Cohen, M.D., Ngan, F., 2015. NOAA's HYSPLIT atmospheric transport and dispersion modeling system. Bull. Am. Meteorol. Soc. 96, 2059–2077. https://doi.org/10.1175/BAMS-D-14-00110.1.
Tegen, I., Schepanski, K., 2009. The global distribution of mineral dust. IOP Conf. Ser. Earth Environ. Sci. 7, 012001. https://doi.org/10.1088/1755-1307/7/1/012001.
Tiwari, S., Kumar, A., Pratap, V., Singh, A.K., 2019. Assessment of two intense dust storm characteristics over Indo – Gangetic basin and their radiative impacts: a case study. Atmos. Res. 228, 23–40. https://doi.org/10.1016/j.atmosres.2019.05.011.
Wang, D., Zhang, F., Yang, S., Xia, N., Ariken, M., 2020. Exploring the spatial-temporal characteristics of the aerosol optical depth (AOD) in Central Asia based on the moderate resolution imaging spectroradiometer (MODIS). Environ. Monit. Assess. 192. https://doi.org/10.1007/s10661-020-08299-x.
Wang, Y.Q., 2014. MeteoInfo: GIS software for meteorological data visualization and analysis. Meteorol. Appl. 21, 360–368. https://doi.org/10.1002/met.1345.
Xi, X., Sokolik, I.N., 2016a. Dust interannual variability and trend in Central Asia from 2000 to 2014 and their climatic linkages. J. Geophys. Res. Atmos. 120, 12175–12197. https://doi.org/10.1002/2015JD024092.
Xi, X., Sokolik, I.N., 2016b. Quantifying the anthropogenic dust emission from agricultural land use and desiccation of the Aral Sea in Central Asia. J. Geophys. Res. Atmos. 121, 12,270–12,281. https://doi.org/10.1002/2016JD025556.
Xi, X., Sokolik, I.N., 2015. Seasonal dynamics of threshold friction velocity and dust emission in Central Asia. J. Geophys. Res. Atmos. 120, 1536–1564. https://doi.org/10.1002/jgrd.v120.410.1002/2014JD022471.
Yu, X., Lü, R., Kumar, K.R., Ma, J., Zhang, Q., Jiang, Y., Kang, N., Yang, S., Wang, J., Li, M., 2016. Dust aerosol properties and radiative forcing observed in spring during 2001–2014 over urban Beijing, China. Environ. Sci. Pollut. Res. 23, 15432–15442. https://doi.org/10.1007/s11356-016-6727-9.
Yu, X., Shi, C., Ma, J., Zhu, B., Li, M., Wang, J., Yang, S., Kang, N., 2013. Aerosol optical properties during firework, biomass burning and dust episodes in Beijing. Atmos. Environ. 81, 475–484. https://doi.org/10.1016/j.atmosenv.2013.08.067.
Zhang, X.X., Claiborn, C., Lei, J.Q., Vaughan, J., Wu, S.X., Li, S.Y., Liu, L.Y., Wang, Z.F., Wang, Y.D., Huang, S.Y., Zhou, J., 2020. Aeolian dust in Central Asia: Spatial distribution and temporal variability. Atmos. Environ. 238, 117734. https://doi.org/10.1016/j.atmosenv.2020.117734.
Zhang, Y., Kang, S., Sprenger, M., Cong, Z., Gao, T., Li, C., Tao, S., Li, X., Zhong, X., Xu, M., Meng, W., Neupane, B., Qin, X., Sillanpää, M., 2018. Black carbon and mineral dust in snow cover on the Tibetan Plateau. Cryosphere 12, 413–431. https://doi.org/10.5194/tc-12-413-2018.